UNCLASSIFIED

Technical Report #46

SECURITY CLASSIFICATION OF THIS PAGE

REPORT DOCUMENTATION PAGE

DTIC FILE COPY

1a. REPORT SECL
NA

1b. RESTRICTIVE MARKINGS
NA

2a SECURITY CL
NA

AD-A203 489

3. DISTRIBUTION / AVAILABILITY OF REPORT
Distribution Unlimited; Approved for Public Release

2b. DECLASSIFIC
NA

4. PERFORMING ORGANIZATION REPORT NUMBER(S)

5. MONITORING ORGANIZATION REPORT NUMBER(S)
NA

DTIC ELECTE 24 JAN 1989

6a. NAME OF PERFORMING ORGANIZATION	6b. OFFICE SYMBOL (If applicable)	7a. NAME OF MONITORING ORGANIZATION
Indiana University	NA	ONR

6c. ADDRESS (City, State, and ZIP Code)	7b. ADDRESS (City, State, and ZIP Code)
Department of Chemistry Bloomington, IN 47405	800 N. Quincy Street Arlington, VA 22217

8a. NAME OF FUNDING / SPONSORING ORGANIZATION	8b. OFFICE SYMBOL (If applicable)	9. PROCUREMENT INSTRUMENT IDENTIFICATION NUMBER
		Contract N00014-86-K-0366

8c. ADDRESS (City, State, and ZIP Code)	10. SOURCE OF FUNDING NUMBERS			
	PROGRAM ELEMENT NO.	PROJECT NO.	TASK NO. R&T Code 4134006	WORK UNIT ACCESSION NO.

11. TITLE (Include Security Classification)
A New Procedure for Determination of Electron Temperatures and Electron Concentrations by Thomson Scattering from Analytical Plasmas

12. PERSONAL AUTHOR(S)
Mao Huang and Gary M. Hieftje

13a. TYPE OF REPORT	13b. TIME COVERED	14. DATE OF REPORT (Year, Month, Day)	15. PAGE COUNT
Technical	FROM _____ TO _____	28 October 1988	39

16. SUPPLEMENTARY NOTATION

17. COSATI CODES			18. SUBJECT TERMS (Continue on reverse if necessary and identify by block number)
FIELD	GROUP	SUB-GROUP	Thomson Scattering, Inductively Coupled Plasma, Multi-element Analysis, Electron Temperatures, Electron Concentrations.

19. ABSTRACT (Continue on reverse if necessary and identify by block number)

A new data-treatment procedure allows for more accurate determination of electron temperatures and electron concentrations in analytical plasmas. A Thomson-scattering spectrum, useful for these determinations, is often not purely Gaussian in shape, even when the probed electrons possess a Maxwellian velocity distribution. Nonetheless, an unambiguous relationship exists between electron temperatures and concentrations that truly exist in a plasma and those calculated from a distorted Thomson-scattering spectrum. Understanding this relationship permits a look-up table to be constructed, from which observed values can be corrected. Theory concerning this procedure is described and details for using it with both a ruby laser and frequency-doubled Nd: YAG laser are discussed. Examples of electron temperature and electron concentration determined with this procedure in an ICP are given. The possibility of using the new procedure to study electron-energy distributions is also assessed. Keywords:

20 DISTRIBUTION / AVAILABILITY OF ABSTRACT	21 ABSTRACT SECURITY CLASSIFICATION
☒ UNCLASSIFIED/UNLIMITED ☐ SAME AS RPT ☐ DTIC USERS	Distribution Unlimited

22a NAME OF RESPONSIBLE INDIVIDUAL	22b TELEPHONE (Include Area Code)	22c OFFICE SYMBOL
Gary M. Hieftje	(812) 335-2189	

DD FORM 1473, 84 MAR 83 APR edition may be used until exhausted
All other editions are obsolete

SECURITY CLASSIFICATION OF THIS PAGE
UNCLASSIFIED

89 1 23 109

A New Procedure for Determination of Electron Temperatures and Electron Concentrations by Thomson Scattering from Analytical Plasmas

Mao Huang* and Gary M. Hieftje+

Department of Chemistry

Indiana University

Bloomington, IN 47405

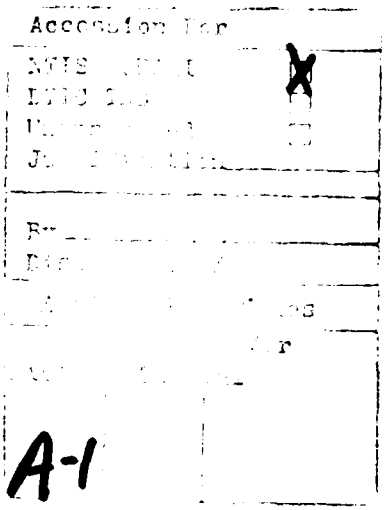

*On leave from:
Department of Physics
The Branch School of Peking University
Beijing, China

+Author to whom correspondence should be addressed.

Abstract -- A new data-treatment procedure allows for more accurate determination of electron temperatures and electron concentrations in analytical plasmas. A Thomson-scattering spectrum, useful for these determinations, is often not purely Gaussian in shape, even when the probed electrons possess a Maxwellian velocity distribution. Nonetheless, an unambiguous relationship exists between electron temperatures and concentrations that truly exist in a plasma and those calculated from a distorted Thomson-scattering spectrum. Understanding this relationship permits a look-up table to be constructed, from which observed values can be corrected. Theory concerning this procedure is described and details for using it with both a ruby laser and frequency-doubled Nd:YAG laser are discussed. Examples of electron temperature and electron concentration determined with this procedure in an ICP are given. The possibility of using the new procedure to study electron-energy distributions is also assessed.

1. INTRODUCTION

The inductively coupled plasma (ICP) has become an extremely important source for analytical atomic emission and mass spectrometry [1]. In such a plasma, electrons are probably the most active and important species, at least as far as energy transfer, excitation and ionization are concerned. It is principally electrons that pick up energy from the rf field generated by the induction coil and transfer it to ions and atoms [2]. In this way, electrons play a prominent role in sustaining the plasma and in transporting energy throughout the discharge [3,4]. As importantly, electrons are involved in most of the events that are considered significant in excitation and ionization of analyte species [5-9]. It is therefore not surprising that electrons have been studied extensively in the ICP [10-24].

Among the methods to investigate electrons, Thomson scattering [25] offers a number of advantages. It provides values for both electron concentration and temperature simultaneously, and can do so on a spatially and temporally resolved basis. Moreover, under proper conditions, it can indicate true electron-energy distributions. Thomson scattering has been used as a diagnostic tool in nuclear-fusion research for more than 20 years [26,27]. More recently, the feasibility and experimental considerations for using Thomson scattering with analytical plasmas were reviewed and discussed [25,28]. Preliminary results from a single-channel scanning device and a multichannel instrument have proven that Thomson scattering can be a powerful tool for probing electron temperatures or energy distributions, and electron concentrations in the ICP [24,29,30].

Unfortunately, interpretation of Thomson-scattering measurements from an ICP is more complicated than those in a fusion plasma. Fusion plasmas normally have rather high electron temperatures (10^2-10^4 eV) and relatively low electron number densities (10^{12}-10^{15} cm^{-3}), so they produce a Gaussian-shaped Thomson-scattering spectrum, centered at the incident laser wavelength, when a Maxwellian velocity distribution of electrons exists [26,27,31]. Consequently, a plot of the natural logarithm of the Thomson-scattering signal versus the square of the wavelength shift produces a straight line, from the slope of which the electron temperature can be calculated [26]. A least-squares linear fit is usually employed in this calculation, since experimental errors usually occur. In addition, the total intensity of Thomson-scattered light can be used to determine the value for a localized electron number density.

Compared to fusion plasmas, analytical plasmas have rather low electron temperatures ($\leq$ 1 eV) and relatively high electron concentrations (10^{14}-10^{16} cm^{-3}). Consequently, a Thomson-scattering spectrum from an ICP theoretically will not have a purely Gaussian shape even if the electrons in the ICP possess a Maxwellian velocity distribution. A large observation angle (approaching backscattering) and a short incident laser wavelength (for example, a frequency-doubled Nd:YAG laser at 532 nm) will make the scattering spectrum approximate a Gaussian, but distortion will not be completely avoided. One can still apply a least-squares fit to a linearized version of such a spectrum to calculate an electron temperature and can use the integrated intensity of the entire spectrum to calculate an electron concentration [24,25,29,30]. However, the distortion of the spectrum from a true Gaussian will then yield an overestimated electron temperature and an underestimated electron number density; the scattering signals in the center

of the spectrum are depressed, and lead to an erroneously low slope and a lower overall intensity of the spectrum.

In the present paper, an improved procedure will be described which serves to extract valid values for electron temperature and electron number density from an experimental Thomson-scattering spectrum. The deviation between these values and those determined in the conventional way has been found to depend on the incident laser wavelength, on the number of spectral intervals (channels) used in the calculation, and on the magnitudes of the true values themselves. Specifically, a longer wavelength of the incident laser, a smaller number of spectral channels, a higher electron number density and a lower electron temperature all lead to a more substantial deviation of conventionally determined electron temperatures and concentrations from their real values. These points will be illustrated by means of data obtained from recent Thomson-scattering measurements on an analytical ICP. Finally, the feasibility of using the new procedure for detecting a non-Maxwellian electron velocity distribution will be assessed.

2. THEORETICAL CONSIDERATIONS

When an intense light beam strikes a plasma, free electrons are accelerated in resonance with the incident electromagnetic field. As a consequence, the oscillating electrons act as miniature sources themselves and emit radiation of their own. This secondary radiation is termed Thomson scattering. When the electrons are in rapid motion, as is certainly the case in a hot, rare-gas plasma, the scattered radiation will be Doppler-shifted and will produce a so-called Thomson-scattering spectrum, from which electron energies and concentrations can be deduced [24,25,29].

Of course, ions experience the same electromagnetic field as do electrons. However, their mass is so large that they are displaced very little and therefore scatter relatively weakly. Nonetheless, ions can under some conditions greatly influence the electron density oscillation, and thereby lead to a change not only in the shape of the Thomson-scattering spectrum but also in the total intensity of scattered light. This influence makes interpretation of a Thomson spectrum difficult and often leads to errors in calculated electron temperature and number-density values.

To see how these errors can be minimized, let us briefly review the quantitative aspects of Thomson scattering. The spatial and frequency (wavelength) distribution of Thomson-scattered light is expressed by the differential scattering cross section σ (k, ω) [26,32]:

$$\sigma(k, \omega) = \sigma_T \cdot S(k, \omega), \tag{1}$$

where

$$\sigma_T = (e^2/m_e c^2)^2 \sin^2 \gamma \tag{2}$$

is the Thomson cross section, S(k, ω) the so-called dynamic form factor, k the differential scattering wave vector [25,26], and ω the frequency shift of the scattered light from the incident-light frequency. In Eqn. (2), e, m_e and c are the charge and mass of an electron and the speed of light, respectively, and γ is the angle between the observation direction and the electric vector of the incident light beam. The maximum scattering signal is produced at an angle equal to 90°.

For a Maxwellian electron-velocity distribution, the dynamic form factor can be decomposed into two terms, the first of which deals with free-electron scattering and the second of which describes the effect of neighboring ions on electron scattering [26,32]:

$$S(k,\omega)\, d\omega = \Gamma_\alpha(X_e)dX_e + Z\left(\frac{\alpha^2}{1+\alpha^2}\right)^2 \Gamma_\beta(X_i)dX_i \quad ; \tag{3}$$

$$\Gamma_\alpha(X_e) = \frac{\exp(-X_e^2)}{\sqrt{\pi}\left|1+\alpha^2 W(X_e)\right|^2} \quad ; \quad \Gamma_\beta(X_i) = \frac{\exp(-X_i^2)}{\sqrt{\pi}\left|1+\beta^2 W(X_i)\right|^2} \quad ; \tag{4}$$

$$X_e = \frac{\omega}{kV_e} \quad ; \quad X_i = \frac{\omega}{kV_i} \quad ; \tag{5}$$

$$\beta^2 = Z\,\frac{\alpha^2}{1+\alpha^2} \cdot \frac{T_e}{T_i} \quad ; \tag{6}$$

$$W(X) = 1 - 2Xe^{-X^2}\int_0^X e^{P^2}dp - i\sqrt{\pi}\,Xe^{-X^2} \quad ; \tag{7}$$

and

$$\alpha = \frac{1}{k\lambda_D} \tag{8}$$

is the scattering parameter. Note from the shape of $\Gamma_\alpha(X_e)$ and $\Gamma_\beta(X_i)$ that $S(k, \omega)$ is the sum of two Gaussians when $\alpha \ll 1$. In Eqns (3) and (6), Z is the charge on the ion. In Eqn (5) X_e and X_i are dimensionless

frequencies, and V_e and V_i are the most probable velocities of the electron and ion, respectively, which can be determined from

$$V_e = \sqrt{\frac{2k_B T_e}{m_e}} \quad \text{and} \quad V_i = \sqrt{\frac{2k_B T_i}{m_i}} \tag{9}$$

where k_B is the Boltzmann constant, T_e and T_i are the electron and ion temperatures, respectively, and m_i is the mass of the ion. In Eqn (8), λ_D is the Debye length given by

$$\lambda_D = \sqrt{\frac{k_B T_e}{4\pi n_e e^2}} \tag{10}$$

where n_e is the electron number density. The Debye length λ_D is a measure of the charge-shielding distance in a plasma [33]. Electrons exhibit individual behavior on a scale much shorter than the Debye length and can be considered free; collective electron motion occurs over a range longer than the Debye length, and results in correlated or coherent phenomena.

The scalar quantity k in Eqns (5) and (8) has to do with the distance in the plasma over which scattering occurs. When a laser beam of wavelength λ_o is incident on a plasma, light scattering at an angle θ with respect to the incident direction occurs on a distance scale of

1/k, where k is the magnitude of the vector quantity k and is given by [26,32]

$$k = \frac{4\pi\sin(\theta/2)}{\lambda_o} \quad . \tag{11}$$

Clearly, when $(1/k)<<\lambda_D$, $\alpha<<1$ (see Eqn (8)), and electrons in the plasma would behave as if they were free in the electromagnetic field of the laser beam. As a result, the spectrum of scattered light would directly reflect the electron-velocity distribution. This behavior can be readily seen from Eqns (3) and (4), because the second term on the right hand side of Eqn (3) can then be neglected, as can the value of $\alpha^2 W(X_e)$ in the first term. Under these conditions,

$$S(k,\omega)\ d\omega = \frac{\exp(-X_e^2)}{\sqrt{\pi}}\ dX_e, \tag{12}$$

which shows that the scattering spectrum will have a Gaussian shape.

Integrating Eqn (12) over frequency ω for the entire spectrum leads to

$$\int_{-\infty}^{\infty} S(k,\omega)\ d\omega = \int_{-\infty}^{\infty} \frac{\exp(-X_e^2)}{\sqrt{\pi}}\ dX_e = 1 \tag{13}$$

Combining Eqns (1) and (13) indicates that the integral of the differential scattering cross section $\sigma\ (k,\omega)$ over frequency becomes equal to the Thomson cross section, when $\alpha<<1$. Therefore, the detected

scattering signal $I(\omega)$ is proportional to $S(\mathbf{k},\omega)$ given by Eqn (12). From this relationship and Eqn (12), one can obtain the following expression by taking a logarithm:

$$\ln I(\omega) = C - X_e^2 = C - \left(\frac{\omega}{kV_e} \right)^2 \qquad (14)$$

where C is a constant. Let us now substitute $\omega = - \frac{2\pi c}{\lambda_o^2} \Delta\lambda$ (where $\Delta\lambda$ is the wavelength shift corresponding to the frequency shift ω), Eqn (9) and Eqn (11) into Eqn (14) to obtain

$$\ln I(\lambda) = C - \frac{m_e c^2}{8 k_B T_e \sin^2 \frac{\theta}{2} \cdot \lambda_o^2} (\Delta\lambda)^2 \qquad (15)$$

From Eqn (15), the slope of a plot of $\ln I(\lambda)$ vs. $(\Delta\lambda)^2$ can be used to determine the electron temperature T_e. This is the usual way to find the electron temperature from a Thomson-scattering spectrum, and is convenient and accurate when $\alpha \ll 1$. Furthermore, under these conditions ($\alpha \ll 1$) the calibrated signal can be used to determine the electron concentration precisely, because the average light-scattering cross section of an electron is simply equal to the Thomson cross section as discussed above. As a result, the absolute scattering intensity is directly proportional to the electron number density.

Errors Resulting from $\alpha \neq 0$

Unfortunately, the condition $\alpha \ll 1$ does not exist in the ICP. For a given electron temperature T_e and electron concentration n_e, a shorter laser wavelength λ_o and larger observation angle θ will produce a smaller α value (cf. Eqns (8) and (11)). However, even for a backscattering geometry ($\theta = 180°$), the wavelength of a ruby laser (694 nm) or a frequency doubled Nd:YAG laser (532 nm) will yield α values that lie between 0.1 and 1. Consequently, the electrons will not behave independently and the scattering spectra will deviate from their ideally Gaussian shape.

Electron-Temperature Errors

The degree of this deviation and its dependence on α are revealed in the curves of Fig. 1 calculated according to Eqns (4) and (7). Interestingly, the curves all nearly cross at about $X_e = 1.0$. At values of X_e below 1.0, the center of each curve is depressed when $\alpha > 0$ and by an amount that increases with α. In contrast, the tail ($X_e > 1.0$) of each spectrum is raised slightly when α is above zero.

Because only the curve in Fig. 1 corresponding to $\alpha = 0$ is Gaussian, plotting of $\ln \Gamma_\alpha(X_e)$ vs. X_e^2 for the other curves results in bending (see Figs. 2 and 3). To construct Figs. 2 and 3, ten values of X_e ranging from 0.2 to 2.0 (separated by 0.2) were used, and correspond roughly to the channels used in a multichannel Thomson-scattering experiment. At each of these values, the quantity $\ln \Gamma_\alpha(X_e)$ was calculated and plotted as circles (Fig. 2) or triangles (Fig. 3). A least-squares linear fit to these plotted points (solid line) can then be compared to the straight line that would have been produced by $\alpha = 0$

(dashed line). It can be seen that the slope of the least-squares linear fit in both Figs. 2 and 3 (solid line) is less steep than that of the plot for $\alpha = 0$ (dashed line). As a consequence, the electron temperature calculated from Eqn (14) would be overestimated. Moreover, the larger the α value, the greater would be the error in computed electron temperature (compare Figs. 2 and 3).

Note that the disparity among the curves in Fig. 1 is relatively smaller in the tail than in the central part. This relationship is clear also in Figs. 2 and 3, especially if one examines the deviations of circles or triangles from the dashed lines. Obviously, using only scattering signals from the tail channels of a Thomson-scattering spectrum results in a least-squares-linear-fit value for electron temperature that is closer to the real electron temperature than that obtained when the entire scattering spectrum is employed [28]. Unfortunately, the scattering intensity decreases so quickly with wavelength shift (see Fig. 1) that the detected signals in far-wing channels are usually very noisy. It is clearly undesirable not to use scattering signals from channels located closer to the incident laser wavelength.

Errors in Electron Number Density

When the scattering parameter α is not nearly zero, as is the case in the ICP, the average light-scattering cross section of an electron is not equal to the Thomson cross section, but rather decreases with the α value itself. From Eqns (1), (3), and (4), one notes that the scattering cross section of an electron when $\alpha > 0$ is smaller than the Thomson cross section by a factor of [25,26]

$$\frac{\int \sigma(k,\omega)\,d\omega}{\sigma_T} = \int_{-\infty}^{\infty} S(k,\omega)\ d\omega = \int_{-\infty}^{\infty} \Gamma_\alpha\ (X_e)\ dX_e$$

$$= \int_{-\infty}^{\infty} \frac{\exp(-X_e^2)\ dX_e}{\sqrt{\pi}\,|1+\alpha^2 W(X_e)|^2} = \frac{1}{1+\alpha^2} \qquad (16)$$

This fraction is therefore equal to the area between the X_e axis and the curve with a specified α value in Fig. 1, over the entire range of X_e. Clearly, the larger the α value, the smaller the area.

Because of this fixed relationship, one could calculate valid numbers for the electron number density, just by using $\sigma = \sigma_T/(1 + \alpha^2)$ instead of σ_T for the average scattering cross section of the electron. The difficulty encountered, however, is that the correct α value is unknown before a real electron temperature and electron concentration have been determined; in turn, the determination of an electron temperature and concentration requires knowledge of the α value.

Correction Procedure

To overcome this cyclic and apparently insoluble problem, we must recognize that there is an unambiguous relationship among a specific electron temperature, an electron concentration, and the α value [see Eqns (8), (10), and (11)]. Moreover, all affect a Thomson-scattering spectrum in well defined ways [see Eqns. (4), (5), and (7)]. Consequently, for every combination of T_e and n_e, there will be a particular α and a specific Thomson-spectrum shape.

Practically, one can proceed by assuming values for T_e and n_e and by calculating from them a number for α. These parameters then permit a complete Thomson-scattering spectrum to be computed and, from it, a least-squares linear fit and an integrated spectrum. The resulting slope and integral can be used as formerly to derive "experimental" representations for T_e and n_e. This computational procedure can be repeated for all anticipated or realistic combinations of electron temperatures and number densities expected in the ICP, to yield a matrix or table that can be employed to equate "experimental" and real values. The table prepared in this way can then be used in reverse, to deduce true or correct values from those originally determined.

3. PREPARATION AND USE OF CORRECTION TABLES

Correction tables such as described above can be computed for specific laser wavelengths, λ_o, adopted observation angles, θ, and particular numbers of detection channels, each of which covers a specified wavelength range. In this way, a correction table can be tailored to an individual experimental arrangement. Table 1 and Table 2 are two examples that have proven useful in our own studies. Table 1 has been computed for a ruby laser excitation source and with each detection channel covering 0.45 nm; Table 2 applies to the use of a frequency-doubled Nd:YAG laser, with each spectral channel covering 0.34 nm. Both tables pertain to an observation angle of 135° and assume that nine spectral channels are used. Although these tables have proven useful in practice, they can, of course, be prepared with finer resolution in both electron temperature and number density. In

situations where signal-to-noise ratio is extremely high, such smaller increments would obviate the need for interpolation.

Effect of Number of Spectral Channels

As indicated earlier, the electron temperature deduced from a Thomson-scattering spectrum is influenced strongly by intensity values on the "wings" of the spectrum, whereas a calculated electron concentration is affected mostly by values near the central maximum of the spectrum. It is therefore not surprising that the number of spectral channels used in a determination of T_e and n_e would affect the two differently, assuming each channel covers the same spectral interval. This behavior is explored in Figs. 4-7. In these Figures, the number of channels that is cited refers to those in the center of the spectrum; however, they begin just beyond the central (Rayleigh) channel, which has been left vacant.

From Figs. 4 and 5, it is apparent that the deviation of an observed T_e from the real T_e decreases rapidly as more channels are used. Also, because it produces a narrower Thomson-scattering spectrum, the frequency-doubled Nd:YAG laser produces a smaller deviation than the ruby laser for any particular number of channels. Not surprisingly, the deviation is very sensitive to electron concentration and is greatest at large n_e.

Figs. 6 and 7 show "experimental" values of n_e calculated as a function of the number of channels used for the same sets of real T_e and n_e as in Figs. 4 and 5. Not surprisingly, the disparity between observed and real n_e values remains almost unchanged when more than 7 channels are used; the signal from the tail channels of the spectrum is

so small that it does not contribute appreciably to the calculated electron concentration (see Fig. 1). Moreover, both the ruby and frequency-doubled Nd:YAG lasers provide about the same accuracy for n_e determination, particularly when n_e is low (see Fig. 7). Importantly, however, the error in deduced n_e (Figs. 6 and 7) is never as low as that in T_e (Figs. 4 and 5), regardless of how many observation channels are employed. This point will be discussed later.

Application of Correction Tables

The above-mentioned procedure for tracing real electron temperatures and concentrations has been applied to some of our recent Thomson-scattering data and has proven effective and useful. Examples are given in Figs. 8 and 9. Experimental conditions used to obtain these data are cited in Table 3. No sample aerosol was used. In Figs. 8 and 9, the open circles represent values calculated simply by using a least-squares linear fit for T_e and the Thomson cross section for n_e. The filled circles are the corresponding values traced using Table 1 (or similar) and should indicate the true electron temperatures and number densities. In both figures, nine spectral channels were used for data obtained at observation heights of 5.0, 7.5, and 10.0 mm above the load coil (ALC); seven and six channels were used for data taken at 12.5 and 15.0 mm ALC, respectively. Fewer channels were employed higher in the plasma because of the lower n_e that exists there; this lower n_e yields a weaker Thomson signal and produces a poorer signal-to-noise ratio in the tail channels of the spectrum.

Figures 8 and 9 indicate that the new correction procedure becomes more important for both T_e and n_e at lower observation heights. The

reason is that the electron number density is quite high at positions low in the plasma and produces a larger α value. In turn, a large α leads to a more serious depression of the central channel signals and a greater distortion of the Thomson spectrum. Interestingly, the corrected data in Figs. 8 and 9 indicate that the electron temperature does not drop as rapidly with observation height as does electron number density. It would seem then that electron temperature is not responsible for causing major changes in the α value in different regions of the ICP. In general, the corrected data in Figs. 8 and 9 are similar to those previously reported [12,13,16,18,19,22]. Although the electron temperatures cited in Fig. 8 are about 20% lower than those by Batal *et al.* [16], their observation height was below ours (2 mm above the load coil) and their input RF power was 1.5 kW (compared to our 1 kW). Also, the electron number densities in Fig. 9 are roughly twice those reported by Caughlin and Blades [18] at low positions in the plasma (5 mm above the load coil), but are in good agreement at higher spatial points (15 mm above the load coil). This disparity might be due to the slightly different torches used in the two studies.

It should be pointed out that Caughlin and Blades used the Vidal, Cooper and Smith tabulations of half-width to deduct their n_e values; if they had used Goode and Deavor's Stark H_β algrithm [34], their n_e would be lower than ours even at an observation height of 15 mm above the load coil.

From the corrected data shown in Figs. 8 and 9, it is clear that the electron temperatures are not as high as were previously thought. In other words, the ICP is probably not very far from LTE, and therefore the close-to-LTE concept is probably useful in evaluating ICP behavior [5,35,36]. In fact, our T_e values are slightly lower than the LTE values determined by our

measured n_e, obtained using the Saha equation. This relationship reflects the recombining character of the plasma, and would lead to lower ion/atom emission-intensity ratios than only n_e-determined LTE conditions would predict, as has been observed by Caughlin and Blades [36].

4. DISCUSSION AND CONCLUSIONS

When electron number density is high, the deviation of conventionally calculated data from real values is large for both T_e and n_e (see Figs. 4, 6, 8, and 9); the depression of the central channels in a Thomson spectrum induced by a large α value clearly influences both T_e and n_e calculations greatly. In contrast, when the electron number density is low, the deviation in calculated T_e is greatly reduced, as can be seen by comparing Figs. 4 and 5 (see also Fig. 8). However, the deviation in n_e is high even at low n_e (compare Figs. 6 and 7, and see also Fig. 9). The reason is that the underestimation of n_e is due not only to the α value, but also to the fact that the contribution of the central (Rayleigh) channel to the Thomson spectrum cannot be accurately assessed. At that wavelength, Rayleigh scattering and stray light are normally so high that their contribution to the observed signal cannot be subtracted. When electron number density is low, the effect of a large α value on an n_e calculation becomes negligible, but the central-channel signal becomes more important. In turn, ignoring the central-channel signal leads again to an underestimation of n_e. Importantly, this error is automatically avoided when the new correction procedure is performed.

Although the experimental precision of our current Thomson scattering measurements is, on the average, around 10%, we feel that the procedure for

tracing a true T_e and n_e described above should be applicable to Thomson-scattering data obtained in most regions of analytical interest in the ICP. Nonetheless, the accuracy of the resulting values still depends on how well the relative sensitivities of different spectral channels have been normalized and how well the absolute intensity of the entire spectrum has been calibrated. For data obtained on a well normalized and calibrated Thomson-scattering apparatus with high signal-to-noise ratio, the new procedure should offer faithful values of the true T_e and n_e. Of course, the new procedure might not be the only way to trace a real T_e and n_e; curve fitting by a computer is an alternative and attractive approach that we are investigating.

Another approach exists for the unambiguous measurement of real T_e and n_e by Thomson scattering, taking advantage of $\alpha \gg 1$ conditions [26,28]. In this method, n_e is measured directly by observing the resonance satellite related to the electron plasma frequency, using the relation

$$\omega^2 = \omega_p^2 \, (1 + 3/\alpha^2) \tag{17}$$

where ω is the satellite peak frequency and ω_p is the electron plasma frequency, which depends only upon the n_e value

$$\omega_p{}^2 = \frac{4\pi n_e e^2}{m_e} \tag{18}$$

At very shallow scattering angles, $\alpha \gg 1$ and $\omega \approx \omega_p$, so n_e can be calculated directly from Eqn. (18). Then at a steeper angle (say 30°), ω can be measured again, permitting α to be computed from Eqn. (17) and T_e to be determined from Eqns. (8), (10), and (11). However, this approach

requires a very small observation angle θ, and at least one additional observation direction for the determination of both T_e and n_e. Consequently, more effective stray light rejection and a more sophisticated experimental arrangement would be necessary than in the present Thomson-scattering system.

Application to Non-Maxwellian Electron Energy Distributions

In most regions of the ICP, a Thomson-scattering spectrum will not have a purely Gaussian shape, and it is appropriate to ask whether such a spectrum can be used to study electron-energy distributions. Indeed it can, but only if the scattering system has been well normalized, and offers a high signal-to-noise ratio.

In an ICP, where the value of α departs substantially from zero, a departure from Maxwellian behavior could be discerned in the following way. First, the "experimental" values of T_e and n_e can be calculated in the conventional manner and the corresponding true values found by performing the procedure suggested in this paper. The theoretical signal magnitude from each channel used in the Thomson-scattering measurements can then be calculated by using the true (corrected) T_e and n_e magnitudes and Eqns (4) and (7). If the electron velocity distribution is Maxwellian, the calculated signal in each spectral channel should be in good agreement with the corresponding measured one. Otherwise, some of the calculated signal intensities would be higher and some would be lower than the corresponding measured data, but the least-squares linear fit should be almost the same for both calculated and measured intensities. Carefully examining how the measured signals

deviate from the calculated intensities would give information about the electron energy distribution in the plasma.

Finally, it should be pointed out that the procedure suggested here for tracing real T_e and real n_e from observed values applies not only to the ICP, but also to any other plasmas with comparable ranges of T_e and n_e.

ACKNOWLEDGEMENT

Supported in part by the National Science Foundation through grant CHE 87-22639, by the Office of Naval Research, by American Cyanamid, and by BP America. The authors wish to thank Dr. W-H. Hsu for valuable computer programming used in this study.

REFERENCES

1. D. S. DOUGLAS and R. S. HOUK, *Prog. Anal. Atom. Spectrosc.* 8, 1 (1985).
2. M. HUANG and G. M. HIEFTJE, Paper #575 at 14th Annual Meeting of the Federation of Analytical Chemistry and Spectroscopy Societies, Detroit, MI, October (1987).
3. V. A. FASSEL and R. N. KNISELEY, *Anal. Chem.* 46, 1155A (1974).
4. S. GREENFIELD, H. McD. McGEACHIN and P. B. SMITH, *Talanta* 22, 553 (1975).
5. D. C. SCHRAM, I.J.M.M. RAAIJMAKERS, B. van der SIJDE, H.J.W. SCHENKELLAARS, and P.W.J.M. BOUMANS, *Spectrochim. Acta* 38B, 1545 (1983).
6. A. BATEL and J. M. MERMET, *Canadian J. Spectrosc.* 27, 37 (1982).
7. G. F. KIRKBRIGHT, *Developments in Atomic Plasma Spectrochemical Analysis*, p. 223, Ed. R. M. BARNES. Hayden, London (1981).
8. G. M. HIEFTJE, J. W. MILLS, J. W. CARR, G. D. RAYSON, M. HUANG, and K. A. MARSHALL, Analytical Chemistry in the Exploration, Mining and Processing of Materials, p. 15, Ed. L.R.P. BUTLER. Blackwell, Oxford (1986).
9. G. D. RAYSON and G. M. HIEFTJE, *Spectrochim. Acta* 41B, 683 (1986).
10. Y. NOJIRI, K. TANABE, H. UCHIDA, K. FUWA, and J. D. WINEFORDNER, *Spectrochim. Acta* 38B, 61 (1983).
11. J. M. MERMET, *Spectrochim. Acta* 30B, 383 (1975).
12. G. R. KORNBLUM and L. de GALAN, *Spectrochim. Acta* 32B, 71 (1977).
13. D. J. KALNICKY, V. A. FASSEL, and R. N. KNISELEY, *Appl. Spectrosc.* 31, 137 (1977).

14. J. JAROSZ, J. M. MERMET, and J. P. ROBIN, *Spectrochim. Acta* 33B, 55 (1978).

15. J. F. ALDER, R. M. BOMBELKA, and G. F. KIRKBRIGHT, *Spectrochim. Acta* 35B, 163 (1980).

16. A. BATAL, J. JAROSZ, and J. M. MERMET, *Spectrochim. Acta* 36B, 983 (1981).

17. M. W. BLADES and B. L. CAUGHLIN, *Spectrochim. Acta* 40B, 579 (1985).

18. B. L. CAUGHLIN and M. W. BLADES, *Spectrochim. Acta* 40B, 987 (1985).

19. E. H. CHOOT and G. HORLICK, *Spectrochim. Acta* 41B, 935 (1986).

20. L. J. PRELL, C. MONNIG, R. E. HARRIS, and S. R. KOIRTYOHANN, *Spectrochim. Acta* 40B, 1401 (1985).

21. A. MONTASER and V. A. FASSEL and G. LARSEN, *Appl. Spectrosc.* 35, 385 (1981).

22. F. AESCHBACH, *Spectrochim. Acta* 37B, 987 (1982).

23. S. R. GOODE and J. P. DEAVOR *Spectrochim. Acta* 39B, 813 (1984).

24. M. HUANG, K. A. MARSHALL, and G. M. HIEFTJE, *Anal. Chem.* 58, 207 (1986).

25. M. HUANG and G. M. HIEFTJE, *Spectrochim. Acta* 40B, 1387 (1985).

26. D. E. EVANS and J. KATZENSTEIN, *Rep. Prog. Phys.* 32, 207 (1969).

27. J. SCHEFFIELD, *Plasma Scattering of Electromagnetic Radiation.* Academic Press, New York (1975).

28. A. SCHEELINE and M. J. ZOELLNER, *Appl. Spectrosc.* 38, 245 (1984).

29. M. HUANG, K. A. MARSHALL, and G. M. HIEFTJE, *Spectrochim. Acta* 40B, 1211 (1985).

30. K. A. MARSHALL and G. M. HIEFTJE, *Spectrochim. Acta* (submitted, 1987).

31. H. J. KUNZE, *Plasma Diagnostics*, Ed. W. LOCHTE-HOLTGREVEN. North-Holland, Amsterdam (1968).

32. E. E. SALPETER, *Phys. Rev.* **120**, 1528 (1960).

33. F. F. CHEN, *Introduction to Plasma Physics*. Academic Press, New York (1974).

34. S. R. GOODE and J. P. DEAVOR, *Spectrochim. Acta* **39B**, 813 (1984).

35. B. L. CAUGHLIN and M. W. BLADES, *Spectrochim. Acta* **40B**, 1539 (1985).

36. J. A. M. van der MULLEN, I. J. M. M. RAAIJMAKERS, A. C. A. P. van LAMMEREN, D. C. SCHRAM, B. van der SIJDE and H. J. W. SCHENKELAARS, *Spectrochim. Acta* **42B**, 1039 (1987).

Table 1. Correction table for ruby-laser source. Real (true) T_e (top line) and N_e (left column) values and corresponding observed (experimental) values (table entries) pertaining to use of a ruby laser and nine 0.45-nm-wide spectral channels. The range of channels cover a wavelength shift (at the center of each channel) from 0.45 to 4.05 nm. Deleted channels listed on the upper-left corner of the table are available in the Thomson-scattering system, but are not used for reasons described in the text.

deleted channels(ruby): 0 10 11 12 13

REAL Ne		REAL Te							
		0.550000E+04	0.600000E+04	0.650000E+04	0.700000E+04	0.750000E+04	0.800000E+04	0.850000E+04	0.900000E+04
0.100000E+16	Te=	0.673258E+04	0.627366E+04	0.681607E+04	0.735938E+04	0.790325E+04	0.844735E+04	0.899142E+04	0.953523E+04
	NE=	0.767741E+15	0.778800E+15	0.788347E+15	0.796598E+15	0.803722E+15	0.809856E+15	0.815113E+15	0.819689E+15
0.150000E+16	Te=	0.686390E+04	0.642791E+04	0.699406E+04	0.756168E+04	0.813018E+04	0.869908E+04	0.926792E+04	0.983637E+04
	NE=	0.109505E+16	0.111463E+16	0.113145E+16	0.114619E+16	0.115902E+16	0.117018E+16	0.117986E+16	0.118821E+16
0.200000E+16	Te=	0.600197E+04	0.659035E+04	0.718178E+04	0.777632E+04	0.837014E+04	0.896552E+04	0.956085E+04	0.101556E+05
	NE=	0.139154E+16	0.142061E+16	0.144602E+16	0.146828E+16	0.148778E+16	0.150486E+16	0.151980E+16	0.153282E+16
0.250000E+16	Te=	0.614713E+04	0.676146E+04	0.737986E+04	0.800111E+04	0.862409E+04	0.924784E+04	0.987153E+04	0.104946E+05
	NE=	0.166130E+16	0.170074E+16	0.173540E+16	0.176592E+16	0.179280E+16	0.181648E+16	0.183731E+16	0.185561E+16
0.300000E+16	Te=	0.629977E+04	0.694177E+04	0.758902E+04	0.823995E+04	0.889313E+04	0.954732E+04	0.102014E+05	0.108546E+05
	NE=	0.190771E+16	0.195803E+16	0.200245E+16	0.204173E+16	0.207650E+16	0.210728E+16	0.213449E+16	0.215851E+16
0.350000E+16	Te=	0.646032E+04	0.713190E+04	0.781005E+04	0.849283E+04	0.917847E+04	0.986540E+04	0.105522E+05	0.112379E+05
	NE=	0.213364E+16	0.219510E+16	0.224959E+16	0.229798E+16	0.234099E+16	0.237921E+16	0.241316E+16	0.244326E+16
0.400000E+16	Te=	0.662930E+04	0.733252E+04	0.804384E+04	0.876089E+04	0.948148E+04	0.102037E+05	0.109258E+05	0.116464E+05
	NE=	0.234150E+16	0.241422E+16	0.247895E+16	0.253665E+16	0.258811E+16	0.263400E+16	0.267491E+16	0.271134E+16
0.450000E+16	Te=	0.680724E+04	0.754440E+04	0.829139E+04	0.904537E+04	0.980369E+04	0.105640E+05	0.113243E+05	0.120827E+05
	NE=	0.253335E+16	0.261733E+16	0.269234E+16	0.275945E+16	0.281947E+16	0.287318E+16	0.292122E+16	0.296414E+16
0.500000E+16	Te=	0.699476E+04	0.776838E+04	0.855381E+04	0.934768E+04	0.101468E+05	0.109484E+05	0.117500E+05	0.125493E+05
	NE=	0.271095E+16	0.280608E+16	0.289134E+16	0.296784E+16	0.303649E+16	0.309810E+16	0.316335E+16	0.320287E+16
0.550000E+16	Te=	0.719253E+04	0.800540E+04	0.883235E+04	0.966941E+04	0.105128E+05	0.113592E+05	0.122056E+05	0.130494E+05
	NE=	0.287581E+16	0.298193E+16	0.307734E+16	0.316319E+16	0.324044E+16	0.330994E+16	0.337244E+16	0.342859E+16
0.600000E+16	Te=	0.740131E+04	0.825652E+04	0.912841E+04	0.100123E+05	0.109039E+05	0.117991E+05	0.126943E+05	0.135865E+05
	NE=	0.302923E+16	0.314614E+16	0.325155E+16	0.334664E+16	0.343242E+16	0.350978E+16	0.357951E+16	0.364230E+16
0.650000E+16	Te=	0.762196E+04	0.852291E+04	0.944355E+04	0.103785E+05	0.113226E+05	0.122710E+05	0.132196E+05	0.141646E+05
	NE=	0.317236E+16	0.329982E+16	0.341503E+16	0.351922E+16	0.361342E+16	0.369857E+16	0.377547E+16	0.384487E+16
0.700000E+16	Te=	0.785639E+04	0.880589E+04	0.977955E+04	0.107701E+05	0.117716E+05	0.127784E+05	0.137864E+05	0.147882E+05
	NE=	0.330618E+16	0.344391E+16	0.356873E+16	0.368184E+16	0.378434E+16	0.387716E+16	0.396114E+16	0.403708E+16
0.750000E+16	Te=	0.810266E+04	0.910695E+04	0.101384E+05	0.111899E+05	0.122644E+05	0.133252E+05	0.143985E+05	0.154829E+05
	NE=	0.343166E+16	0.357930E+16	0.371347E+16	0.383533E+16	0.394595E+16	0.404630E+16	0.413728E+16	0.421967E+16
0.800000E+16	Te=	0.836494E+04	0.942776E+04	0.105224E+05	0.116408E+05	0.127748E+05	0.139161E+05	0.150582E+05	0.161947E+05
	NE=	0.354927E+16	0.370671E+16	0.385001E+16	0.398039E+16	0.409897E+16	0.420671E+16	0.430454E+16	0.439328E+16
0.850000E+16	Te=	0.864354E+04	0.977020E+04	0.109342E+05	0.121261E+05	0.133366E+05	0.145562E+05	0.157768E+05	0.169910E+05
	NE=	0.365998E+16	0.382684E+16	0.397900E+16	0.411770E+16	0.424403E+16	0.435900E+16	0.446354E+16	0.455850E+16
0.900000E+16	Te=	0.893992E+04	0.101364E+05	0.113767E+05	0.126499E+05	0.139462E+05	0.152517E+05	0.165597E+05	0.178604E+05
	NE=	0.376430E+16	0.394027E+16	0.410104E+16	0.424782E+16	0.438172E+16	0.450374E+16	0.461483E+16	0.471587E+16
0.950000E+16	Te=	0.925570E+04	0.105289E+05	0.118533E+05	0.132167E+05	0.146065E+05	0.160133E+05	0.174157E+05	0.188129E+05
	NE=	0.386275E+16	0.404754E+16	0.421665E+16	0.437128E+16	0.451254E+16	0.464143E+16	0.475890E+16	0.486587E+16

Table 2. Correction table for Nd/YAG laser. Real (true) T_e (top line) and N_e (left column) values and corresponding observed (experimental) values (table entries) pertaining to use of a frequency-doubled Nd:YAG laser, and nine 0.34-nm-wide spectral channels, covering a wavelength shift (at the center of each channel) from 0.39 to 3.08 nm. Deleted channels listed on the upper left corner of the table are available in the Thomson-scattering system, but are not used for reasons described in the text.

deleted channels(YAG): 0 10 11 12 13

REAL Ne		REAL Te							
		0.550000E+04	0.600000E+04	0.650000E+04	0.700000E+04	0.750000E+04	0.800000E+04	0.850000E+04	0.900000E+04
0.100000E+16	Te=	0.581771E+04	0.613993E+04	0.646296E+04	0.678655E+04	0.711052E+04	0.743469E+04	0.775890E+04	0.808303E+04
	Ne=	0.782712E+15	0.773045E+15	0.781997E+15	0.789760E+15	0.796488E+15	0.802303E+15	0.807305E+15	0.811582E+15
0.150000E+16	Te=	0.568514E+04	0.621952E+04	0.675515E+04	0.729168E+04	0.782879E+04	0.836621E+04	0.890371E+04	0.944108E+04
	Ne=	0.111129E+16	0.112851E+16	0.114348E+16	0.115651E+16	0.116786E+16	0.117773E+16	0.118629E+16	0.119366E+16
0.200000E+16	Te=	0.575467E+04	0.630161E+04	0.685028E+04	0.740021E+04	0.795093E+04	0.850209E+04	0.905336E+04	0.960446E+04
	Ne=	0.144033E+16	0.146531E+16	0.148711E+16	0.150617E+16	0.152283E+16	0.153739E+16	0.155007E+16	0.156108E+16
0.250000E+16	Te=	0.582635E+04	0.638627E+04	0.694845E+04	0.751224E+04	0.807709E+04	0.864250E+04	0.920805E+04	0.977339E+04
	Ne=	0.175133E+16	0.178483E+16	0.181415E+16	0.183986E+16	0.186242E+16	0.188220E+16	0.189952E+16	0.191463E+16
0.300000E+16	Te=	0.590023E+04	0.647358E+04	0.704973E+04	0.762791E+04	0.820741E+04	0.878762E+04	0.936801E+04	0.994813E+04
	Ne=	0.204570E+16	0.208830E+16	0.212570E+16	0.215860E+16	0.218755E+16	0.221303E+16	0.223542E+16	0.225504E+16
0.350000E+16	Te=	0.597636E+04	0.656360E+04	0.715426E+04	0.774736E+04	0.834207E+04	0.893764E+04	0.953345E+04	0.101289E+05
	Ne=	0.232466E+16	0.237686E+16	0.242281E+16	0.246333E+16	0.249911E+16	0.253068E+16	0.255852E+16	0.258301E+16
0.400000E+16	Te=	0.605477E+04	0.665643E+04	0.726211E+04	0.787071E+04	0.848123E+04	0.909279E+04	0.970462E+04	0.103161E+05
	Ne=	0.258937E+16	0.265155E+16	0.270642E+16	0.275494E+16	0.279788E+16	0.283589E+16	0.286950E+16	0.289916E+16
0.450000E+16	Te=	0.613556E+04	0.675215E+04	0.737343E+04	0.799814E+04	0.862511E+04	0.925329E+04	0.988180E+04	0.105099E+05
	Ne=	0.284084E+16	0.291330E+16	0.297740E+16	0.303422E+16	0.308462E+16	0.312935E+16	0.316900E+16	0.320410E+16
0.500000E+16	Te=	0.621878E+04	0.685085E+04	0.748835E+04	0.812980E+04	0.877388E+04	0.941937E+04	0.100653E+05	0.107106E+05
	Ne=	0.308002E+16	0.316299E+16	0.323655E+16	0.330190E+16	0.336001E+16	0.341169E+16	0.345762E+16	0.349839E+16
0.550000E+16	Te=	0.630452E+04	0.695265E+04	0.760700E+04	0.826588E+04	0.892777E+04	0.959130E+04	0.102553E+05	0.109187E+05
	Ne=	0.330776E+16	0.340140E+16	0.348461E+16	0.355869E+16	0.362470E+16	0.368352E+16	0.373592E+16	0.378254E+16
0.600000E+16	Te=	0.639283E+04	0.705765E+04	0.772952E+04	0.840656E+04	0.908702E+04	0.976935E+04	0.104522E+05	0.111344E+05
	Ne=	0.352485E+16	0.362926E+16	0.372224E+16	0.380520E+16	0.387926E+16	0.394539E+16	0.400442E+16	0.405705E+16
350000E+16	Te=	0.648382E+04	0.716598E+04	0.785609E+04	0.855203E+04	0.925186E+04	0.995381E+04	0.106564E+05	0.113582E+05
	Ne=	0.373198E+16	0.384724E+16	0.395009E+16	0.404202E+16	0.412425E+16	0.419782E+16	0.426360E+16	0.432237E+16
0.700000E+16	Te=	0.657757E+04	0.727775E+04	0.798686E+04	0.870252E+04	0.942256E+04	0.101450E+05	0.108681E+05	0.115904E+05
	Ne=	0.392982E+16	0.405595E+16	0.416872E+16	0.426970E+16	0.436019E+16	0.444128E+16	0.451392E+16	0.457894E+16
0.750000E+16	Te=	0.667417E+04	0.739312E+04	0.812201E+04	0.885825E+04	0.959940E+04	0.103433E+05	0.110879E+05	0.118316E+05
	Ne=	0.411897E+16	0.425595E+16	0.437866E+16	0.448874E+16	0.458754E+16	0.467623E+16	0.475581E+16	0.482715E+16
0.800000E+16	Te=	0.677374E+04	0.751221E+04	0.826175E+04	0.901947E+04	0.978269E+04	0.105489E+05	0.113161E+05	0.120822E+05
	Ne=	0.429997E+16	0.444777E+16	0.458042E+16	0.469961E+16	0.480676E+16	0.490309E+16	0.498966E+16	0.506740E+16
0.850000E+16	Te=	0.687838E+04	0.763518E+04	0.840626E+04	0.918644E+04	0.997276E+04	0.107624E+05	0.115531E+05	0.123427E+05
	Ne=	0.447332E+16	0.463189E+16	0.477445E+16	0.490274E+16	0.501825E+16	0.512226E+16	0.521586E+16	0.530003E+16
0.900000E+16	Te=	0.698220E+04	0.776220E+04	0.855578E+04	0.935944E+04	0.101699E+05	0.109842E+05	0.117995E+05	0.126137E+05
	Ne=	0.463950E+16	0.480875E+16	0.496117E+16	0.509854E+16	0.522241E+16	0.533410E+16	0.543474E+16	0.552538E+16
0.950000E+16	Te=	0.709134E+04	0.789345E+04	0.871053E+04	0.953877E+04	0.103748E+05	0.112146E+05	0.120558E+05	0.128957E+05
	Ne=	0.479893E+16	0.497877E+16	0.514097E+16	0.528739E+16	0.541960E+16	0.553896E+16	0.564666E+16	0.574377E+16

Table 3. ICP operating conditions

Torch	Commercial MAK torch
RF frequency	27.12 MHz
RF input power	1.0 kw
Outer argon flow	10 l/min
Intermediate argon flow	0.5 l/min
Central flow	0.5 l/min
Sample flow rate	none

Figure Captions

Figure 1. Calculated function $\Gamma_\alpha(X_e)$ for several values of the scattering parameter α. The magnitude of $\Gamma_\alpha(X_e)$ is roughly proportional to the expected spectral intensity of Thomson scattering. For a given experimental system and scattering geometry, X_e is proportional to frequency shift from that of the incident laser (see Eqns (3) (4), and (7)).

Figure 2. Effect of non-Gaussian Thomson-scattering spectrum on errors produced by a linear-fitting process. Calculated values of ln $\Gamma_\alpha(X_e)$ for $\alpha = 0.3$: filled circles; least-squares linear fit of the calculated points: solid line; calculated function ln $\Gamma_\alpha(X_e)$ for $\alpha = 0$: dashed line.

Figure 3. Effect of non-Gaussian Thomson-scattering spectrum on errors produced by a linear-fitting process. Calculated values of ln $\Gamma_\alpha(X_e)$ for $\alpha = 0.5$: filled triangles; least-squares linear fit of the calculated points: solid line; calculated function ln $\Gamma_\alpha(X_e)$ for $\alpha = 0$: dashed line.

Figure 4. "Experimental" electron temperatures calculated as a function of the number of spectral channels used: open circles for ruby laser; filled circles for frequency-doubled Nd:YAG laser. A real $T_e = 8000$ K (dashed line) and a real $N_e = 3 \times 10^{15}$ cm^{-3} are assumed. Number of

channels corresponds to the width of observed spectrum: each channel is 0.45 nm in the case of the ruby laser and 0.34 nm for the Nd:YAG laser.

Figure 5. "Experimental" electron temperatures calculated as a function of the number of spectral channels used: open circles for ruby laser; filled circles for frequency-doubled Nd:YAG laser. A real T_e = 6000 K (dashed line) and a real $n_e = 10^{15}$ cm^{-3} are assumed. Number of channels corresponds to the width of observed spectrum: each channel is 0.45 nm in the case of the ruby laser, and 0.34 nm for the YAG laser.

Figure 6. "Experimental" electron concentrations calculated as a function of the number of spectral channels used: open circles for ruby laser; filled circles for frequency-doubled Nd:YAG laser. A real T_e = 8000 K and a real $n_e = 3 \times 10^{15}$ cm^{-3} (dashed line) are assumed. Number of channels corresponds to the width of observed spectrum: each channel is 0.45 nm in the case of the ruby laser, and 0.34 nm for the YAG laser.

Figure 7. "Experimental" electron concentrations calculated as a function of the number of spectral channels used: open circles for both ruby laser and frequency-doubled Nd:YAG laser. A real T_e = 6000 K and $n_e = 10^{15}$ cm^{-3} (dashed line) are assumed. Number of channels corresponds to the

width of observed spectrum: each channel is 0.45 nm in the case of the ruby laser, and 0.34 nm for the YAG laser.

Figure 8. Electron temperatures T_e measured by Thomson scattering from an ICP at different observation heights and at 3 mm off the plasma axis. Open circles: observed values; filled circles: traced values (see text for detail). ICP operating power - 1 kW; no aerosol is being introduced. See Table 3 for other operating conditions.

Figure 9. Electron concentrations n_e measured by Thomson scattering from an ICP at different observation heights and at 3 mm off the plasma axis. Open circles: observed values; filled circles: traced values (see text for detail). ICP operating power - 1 kW; no aerosol is being introduced. See Table 3 for other operating conditions.

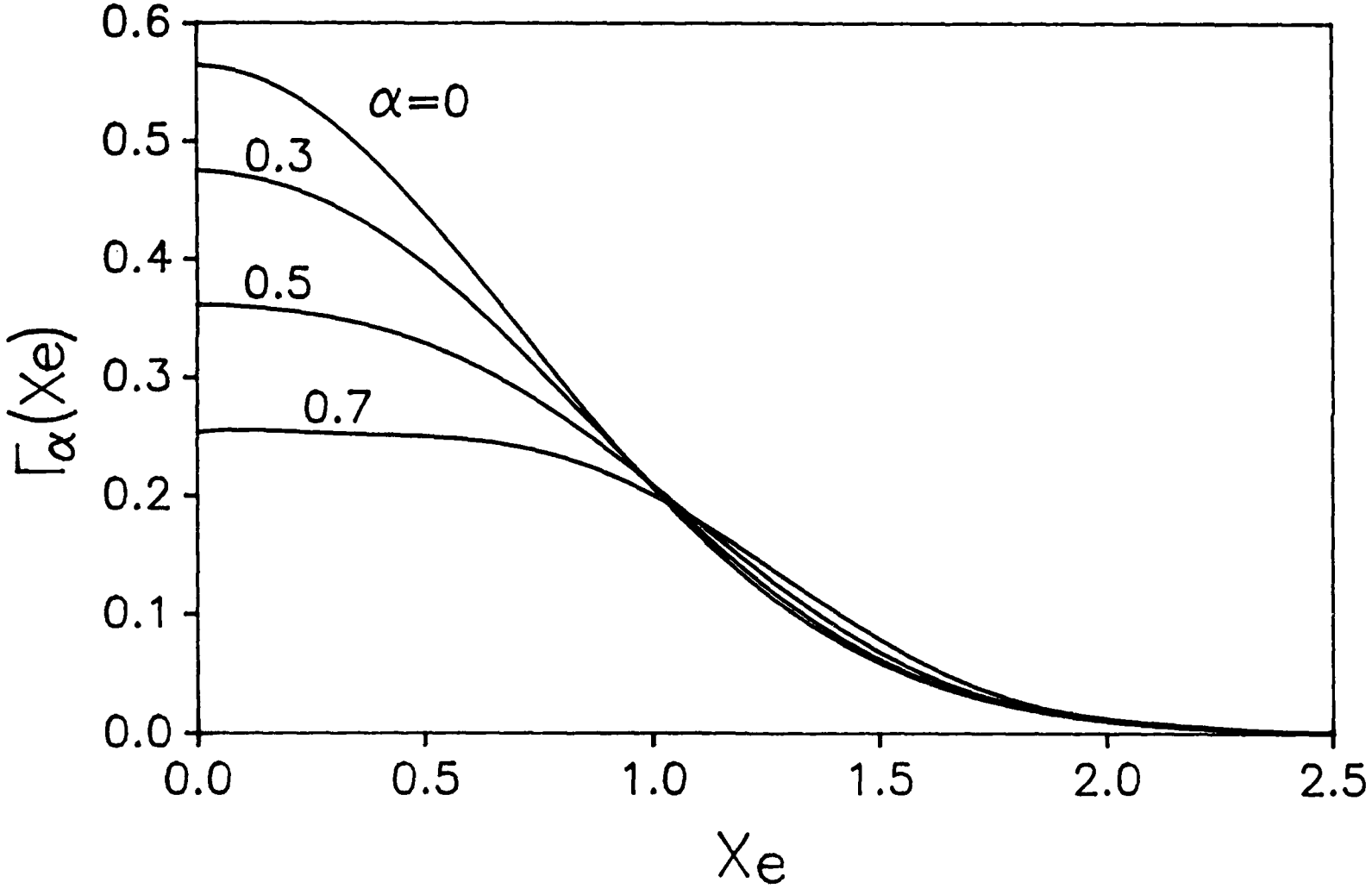

Fig. 1

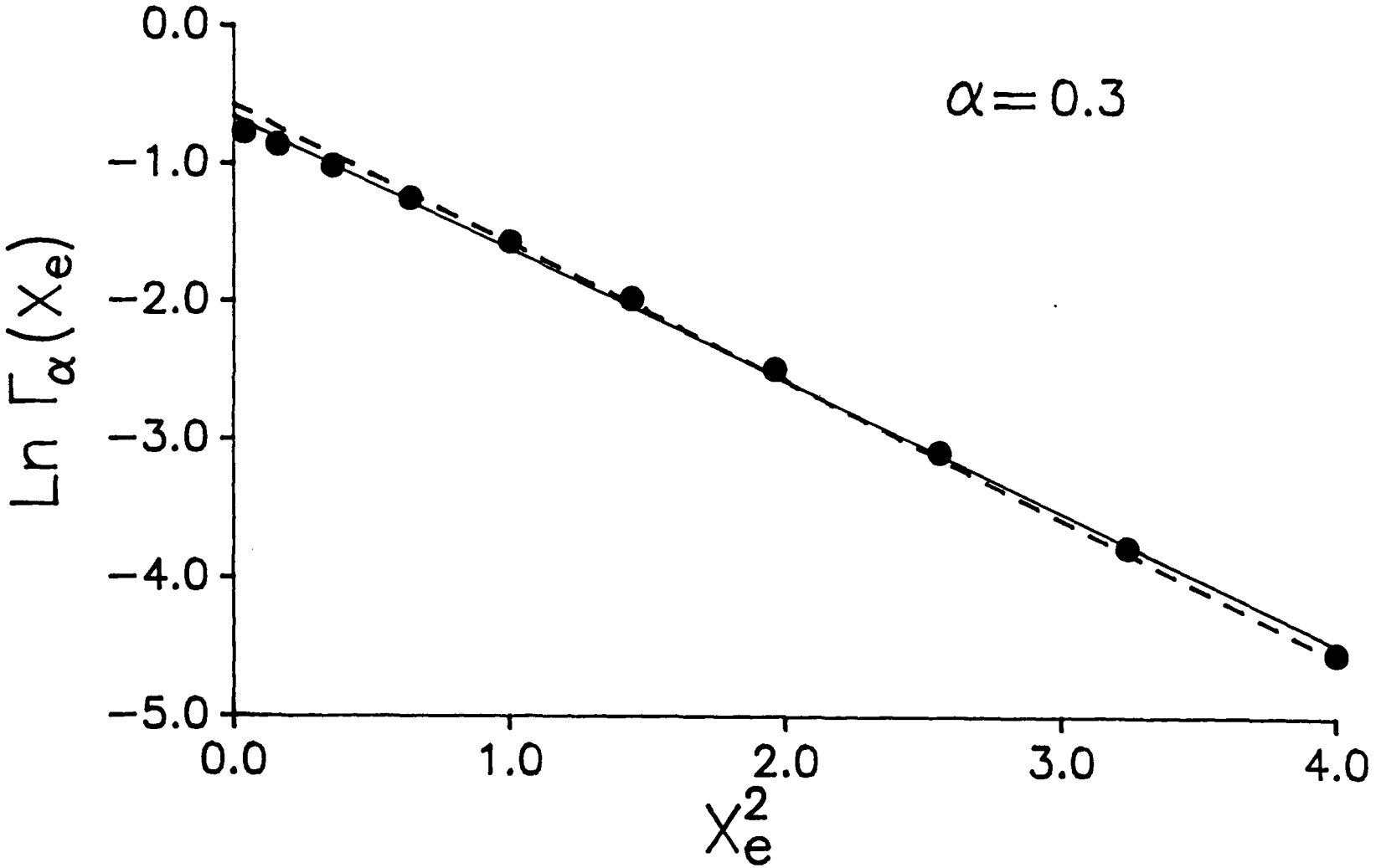

Fig. 2

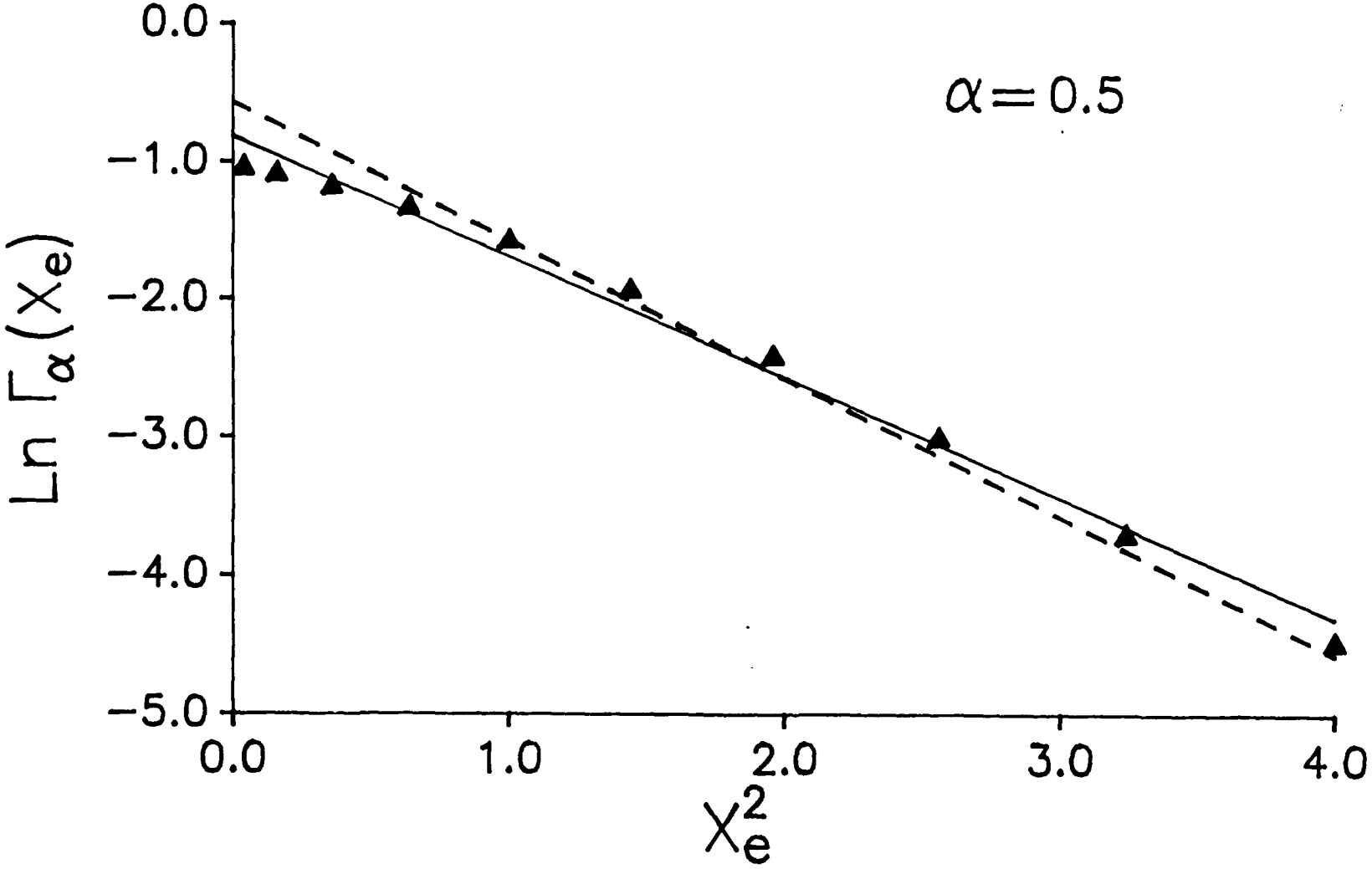

Fig. 3

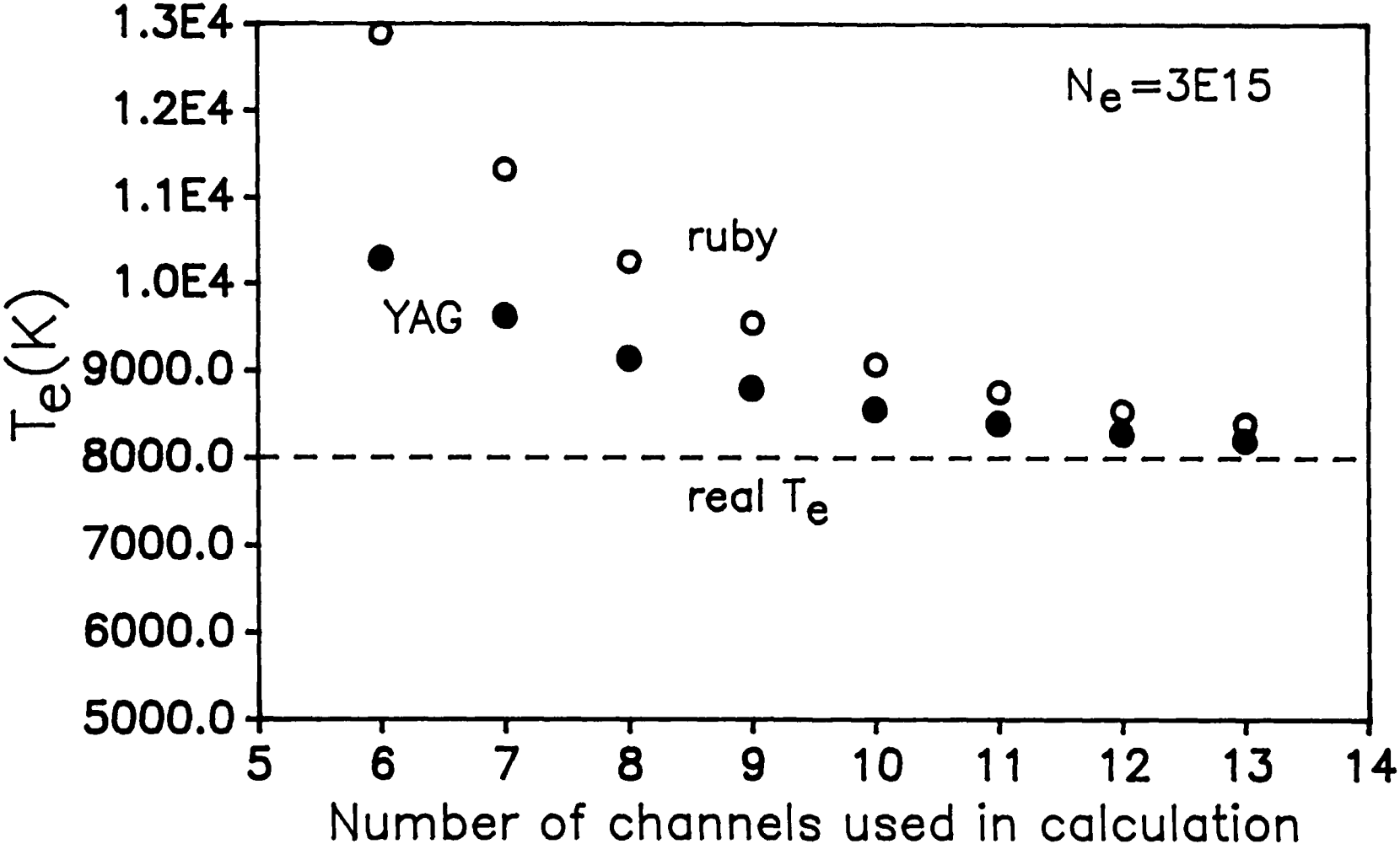
1.3E4
1.2E4
1.1E4
1.0E4
9000.0
8000.0
7000.0
6000.0
5000.0
T_e(K)
N_e=3E15
ruby
YAG
real T_e
5
6
7
8
9
10
11
12
13
14
Number of channels used in calculation

Fig. 4

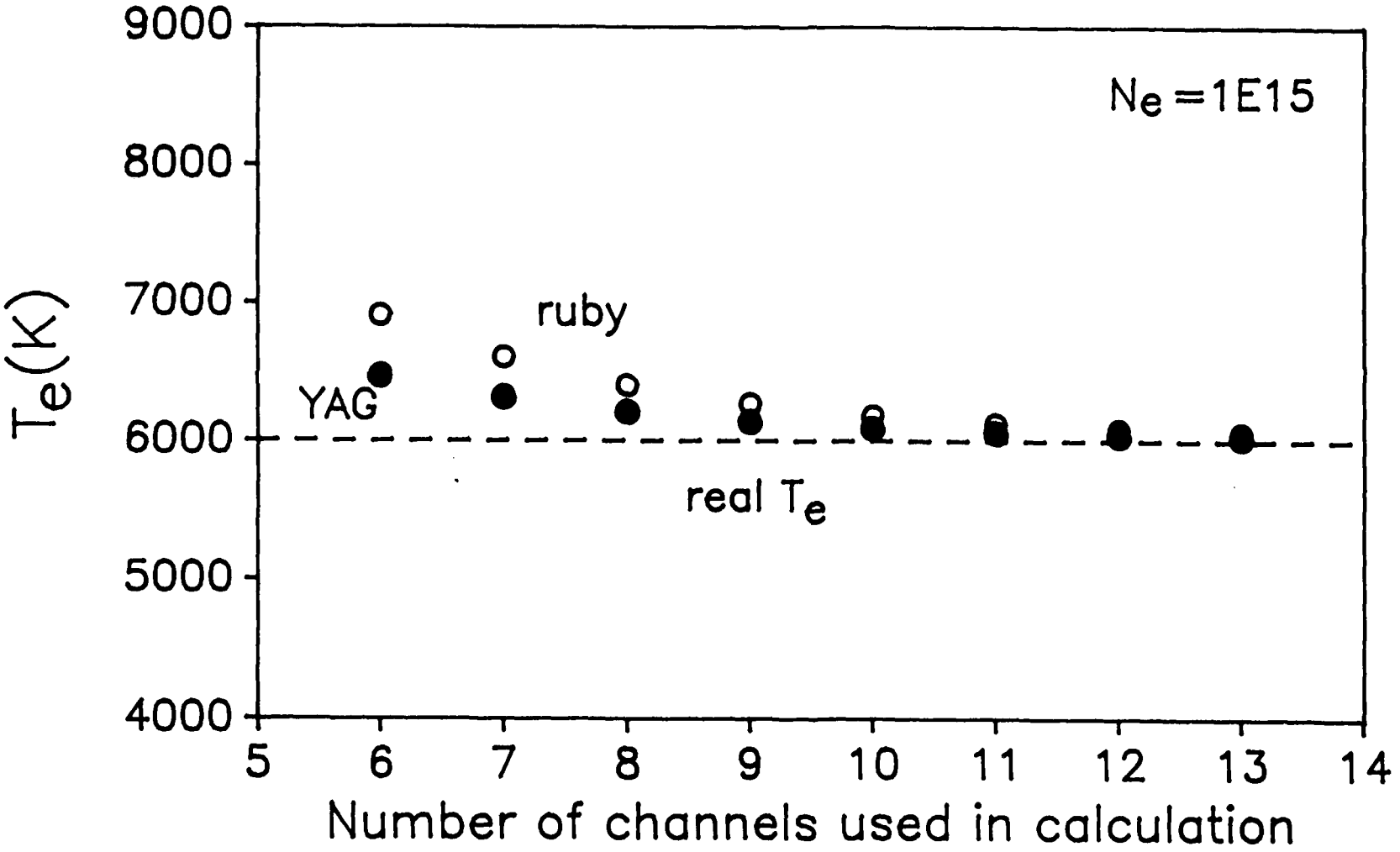
9000
8000
7000
6000
5000
4000
T_e(K)
N_e =1E15
ruby
YAG
real T_e
5
6
7
8
9
10
11
12
13
14
Number of channels used in calculation

Fig. 5

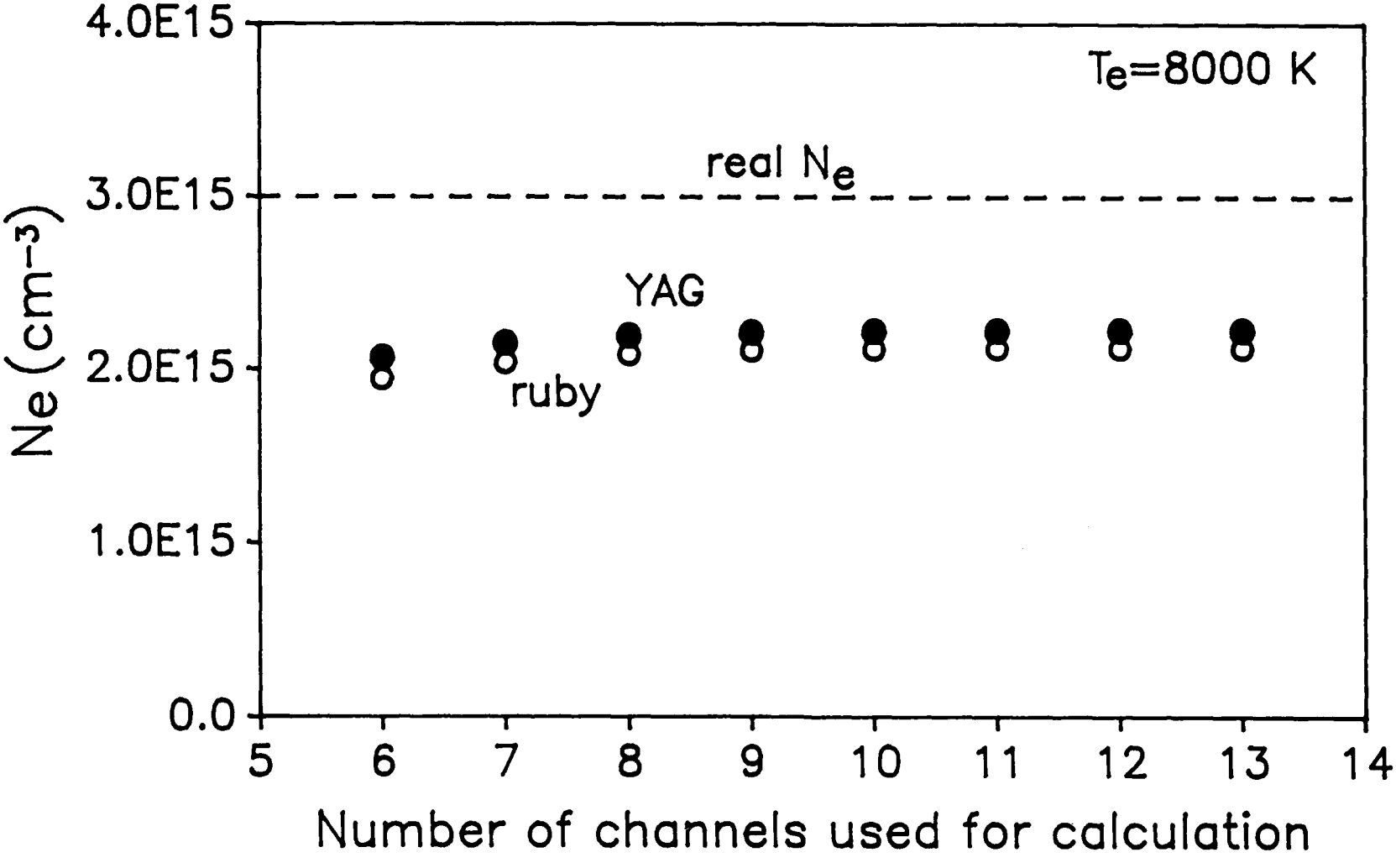
4.0E15
3.0E15
2.0E15
1.0E15
0.0
Ne (cm-3)
Te=8000 K
real Ne
YAG
ruby
5
6
7
8
9
10
11
12
13
14
Number of channels used for calculation

Fig. 6

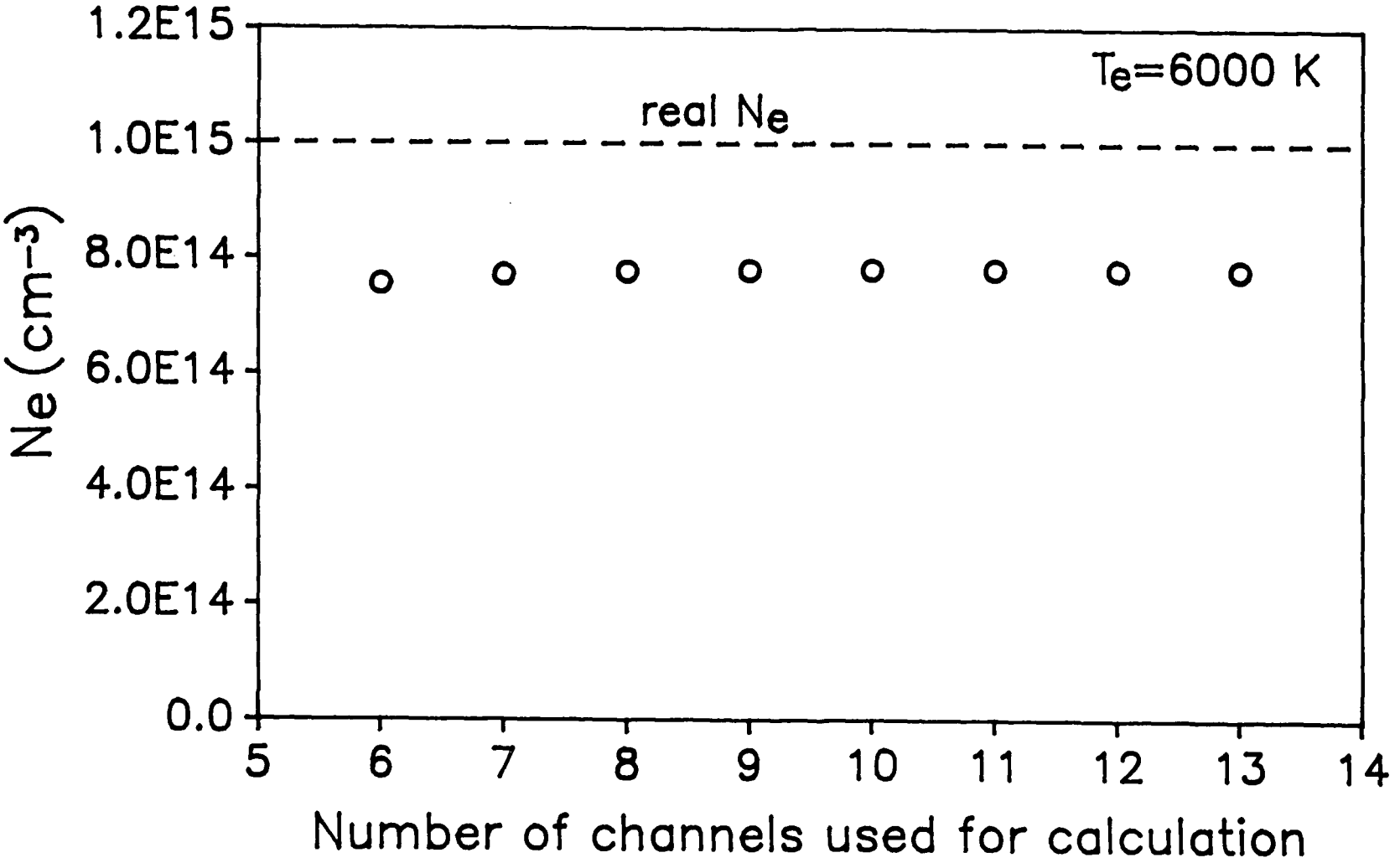
1.2E15
1.0E15
8.0E14
6.0E14
4.0E14
2.0E14
0.0
Ne (cm⁻³)
Te=6000 K
real Ne
5
6
7
8
9
10
11
12
13
14
Number of channels used for calculation

Fig. 7

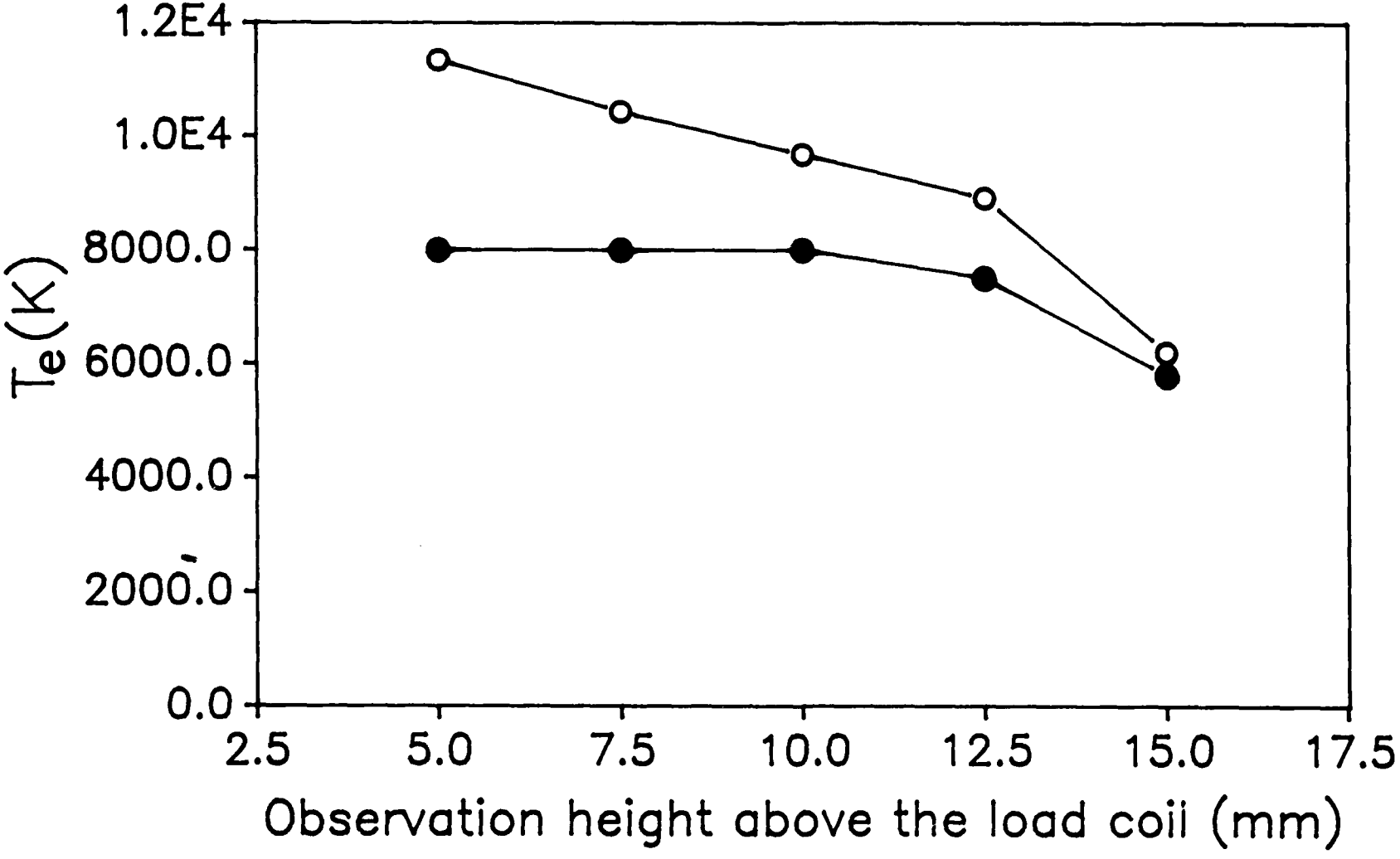
1.2E4
1.0E4
8000.0
6000.0
4000.0
2000.0
0.0
Te(K)
2.5
5.0
7.5
10.0
12.5
15.0
17.5
Observation height above the load coil (mm)

Fig. 8

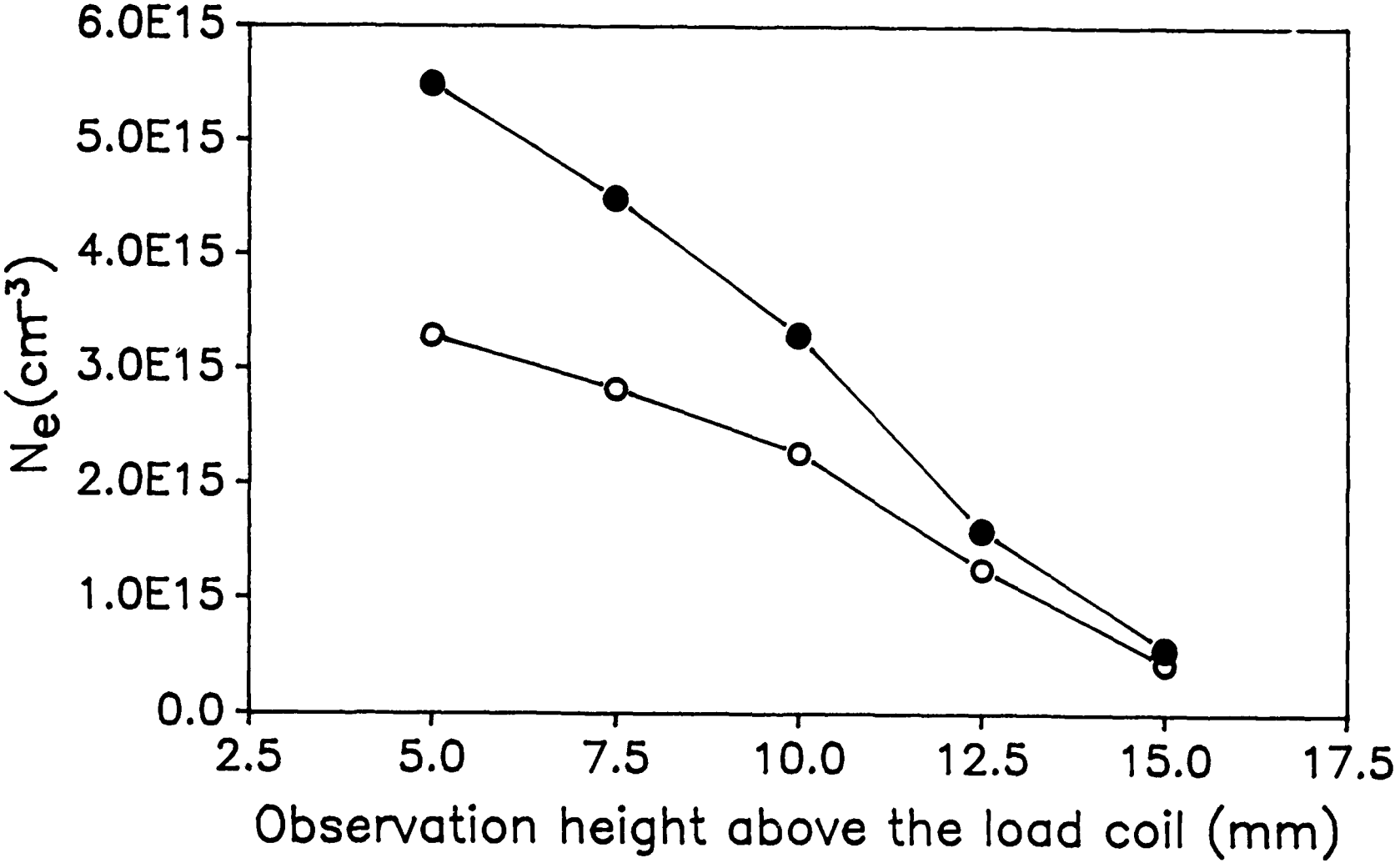
6.0E15
5.0E15
4.0E15
3.0E15
2.0E15
1.0E15
0.0
Ne(cm-3)
2.5
5.0
7.5
10.0
12.5
15.0
17.5
Observation height above the load coil (mm)

Fig. 9